THE JOURNAL OF PHYSICAL CHEMISTRY B

Article

pubs.acs.org/JPCB

Coarse-Grained Molecular Dynamics Simulations of the Phase Behavior of the 4-Cyano-4′-pentylbiphenyl Liquid Crystal System

Jianguo Zhang, Jiaye Su, Yanping Ma, and Hongxia Guo*

Beijing National Laboratory for Molecular Sciences, State Key Laboratory of Polymer Physics and Chemistry, Institute of Chemistry, Chinese Academy of Sciences, Beijing 100190, China

Supporting Information

ABSTRACT: In this paper, with the aim to establish a rational coarse-grained (CG) model for the 4-cyano-4′-pentylbiphenyl (5CB) molecule, we construct three possible CG models (5P, 6P, and 7P) and then determine the bonded and nonbonded interaction parameters separately. For the intramolecular bonded interactions, the bond and angle distributions of the 5CB bulk phase are used as the target properties. For the nonbonded interactions between CG particles, we combine the structure-based and thermodynamic quantities-based methods for the parametrization of CG interaction potentials and attempt to use several fragment molecular systems to derive the CG nonbonded interaction parameters in order to maintain the transferability of our CG models to some extent. Finally, we fix the optimal nonbonded LJ parameters between CG bead pairs such that the results from CG simulations not only correctly reproduce the experimental density and the nematic LC state at 300 K and 1 atm but also reasonably approximate the local structural properties calculated from the underlying atomistic model. Through comparison of the resulting CG data with target properties, the 6P model is found to be the best one among the three, and then we use this model to investigate the phase behavior and dynamic properties. Our results show that the phase transition temperature from nematic to isotropic phase and the diffusion coefficients are reproduced very well, demonstrating the rationality of the 6P model. Our coarse-grained process should have implications for constructing CG models for nCB series or molecules with similar architectures.

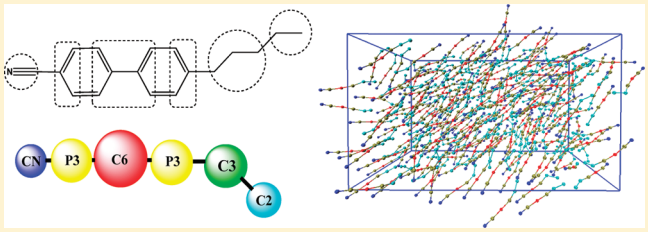

1. INTRODUCTION

5CB (4-cyano-4′-pentylbiphenyl), as a kind of thermotropic liquid crystal (LC) material, has been widely used in various advanced electro-optical device or photonic materials,[1−4] due to the fact that its nematic ordering occurs at the normal temperature. In recent years, considerable experimental efforts[5−14] have been made to study the thermodynamics, dynamics, and phase behavior of 5CB systems. The formation of liquid crystal phases is the essential feature of LC molecules, which is directly related to their industrial applications. Therefore understanding the microscopic origins of such unique phases is of both fundamental and applied interest. But until now, our knowledge on the relationship between microscopic chemical details and the corresponding phase behavior at a molecular level is still rather limited, although such detailed features are known to strongly influence the stability of particular LC phases. Molecular dynamics (MD) simulations have been proven to be very powerful tools for elucidating this relationship, and a number of MD simulations dealing with the 5CB system have been conducted using atomistic models.[15−18] Although some of them could reveal phase transformations, unfortunately, they require a large amount of computational resources. In fact, the phase transitions in LCs involving collective motions often take place within the mesoscopic level spanning, i.e., a spatial scale of $\sim 10^1$ nm and a temporal scale of $\sim 10^2$ ns, which are not easily accessible by conventional atomistic MD simulations. For instance, to determine the phase stability of its homologue 8CB in a typical system with 1024 8CB molecules, our previous atomistic simulations[18] showed that it takes more than 20 days to extend the simulation time over 100 ns using a node with two four-core Intel E5430 CPUs. In contrast, the use of coarse-grained (CG) models constructed from realistic atomistic models in a systematic way can alleviate this problem. Since in such systematic CG models, to arrive at a good but reduced representation of a real system, one merges groups of atoms into a fewer number of CG particles, this reduction in the degrees of freedom of molecules could yield a computational speedup, which considerably enhances our ability to access the phase behavior of 5CB by molecular simulations.

The CG molecular model is considered as a bridge between the *micro*- and the *meso*scope in length and time scales and has been successfully utilized in various systems such as biomolecules[19−22] and polymers[23−31] systems. In general, one should employ different coarse-graining approaches and construct different CG models according to the target properties wanted to be reproduced. However, in most of the previous literature of CG simulations, the procedure of determining suitable force field parameters has been emphasized, and how to

Received: November 9, 2011
Revised: January 10, 2012
Published: January 14, 2012

construct a rational mapping scheme is rarely discussed. In fact, the model always plays a crucial role in the resulting molecular conformations and phase stability. For example, Harmandaris[24] found that the local conformations and melt structures of polystyrene (PS) are clearly different for two similar CG models, in which each PS monomer is presented by two CG beads (in one CG model, one bead represents phenyl group, and the other bead represents the rest; in another CG model, one bead represents phenyl and CH group, and the other bead represents the rest). Van Der Vegt et al.[32] pointed out that there does not exist a formal way to map a given set of atoms into a coarser description, which should depend on the specific system under study. This is especially true for the 5CB molecular system in this work. Compared to the common polymers such as polyethylene (PE), polypropylene (PP), and polybutene (PB), which can be modeled into just one or two types of CG particles, 5CB is a small molecule according to its mass, but its structure is more complex, as 5CB is composed of a rigid biphenyl mesogenic unit with a polar cyano head and a soft short alkyl chain, implying a complex systematic CG process.

So far, several different coarse-graining techniques have been proposed to develop the force field (FF) parameters recently. According to the reproduced properties, these coarse-graining methods can be classified into structure-based[23−26,29−31,33,34] (which aims at reproducing a set of radial distribution functions (RDFs)), force-based[19,35] (monomer interactions), and thermodynamic quantities-based[20−22,36−38] (density, free energy, or interface tension, respectively) ones. Furthermore, two kinds of potential forms, i.e., analytical and tabulated potentials, are often chosen for the interactions between CG particles. Compared to the numerically derived tabulated potentials, the parameters of analytical potentials have clear physical meanings. Also, the analytical potentials have been successfully used in many systems. For example, Marrink[20,37,38] used the standard Lennard-Jones (LJ) 12−6 function for all nonbonded interactions between CG particles to study a wide variety of lipids and proteins, as well as carbohydrates. Srinivas[27] constructed a CG model for diblock copolymers by using a softer LJ 9−6 potential for nonbonded interactions. Kremer's group[23,24,34] chose soft repulsive LJ 7−x (x = 6, 5, or 4) potentials for the CG polystyrene system and Morse potentials for 8AB8 liquid crystalline, respectively. Hence, to keep CG model simple, we will use this rather common form of LJ 9−6 potential for the interactions between CG particles in this paper. Generally, no matter what our choice is, we should hold the same aim at achieving a simpler description of the interactions while minimizing the losses in the applicability or capability of the CG models to predict the properties of interest.[25] Although these coarse-graining methods can reproduce the target properties very well, it is not clear whether they are equally well suited to reproduce other properties.[39] Moreover, it deserves noting that recent novel developments have been motivated toward optimizing the coarse-grained potential to reproduce multiproperties (e.g., several key structural and thermodynamic properties) with the aim to design a coarse-grained model which is thermodynamically and structurally consistent.[40,41] This consistency is of great importance for bridging between the different scales and allowing interchanges between different levels of resolution in a multiscale simulation.[42,43] Considering the case of studying phase transitions, which are accompanied with the variations of density and structural properties, if we want the CG model to display phase transitions approximately at the same temperature and pressure as the underlying atomistic model, the density and structural properties of the nematic phase at normal conditions (i.e., at temperature of 300 K and pressure of 1 atm) can be used as targets for deriving the CG potentials, namely a multiproperty parametrization process.

The main focus of the present work is to build a coarse-grained model for the liquid crystalline 5CB molecule that enables MD simulation study of phase behavior currently almost inaccessible by atomistic models. Since the mapping of an atomistic structure into the CG model is not unique, we have to test various options in order to identify the most appropriate CG model. Given the structural features of the 5CB molecule, that is, a biphenyl mesogenic unit with a cyano head joined to a short soft aliphatic tail, the very straightforward CG models would seem to represent the 5CB molecule as a sequence of spherical beads of different types. Consequently, three different but closely related CG models, i.e., 5P, 6P, and 7P, are proposed, in which the main difference is that the rigid biphenyl group is mapped into the different numbers of CG beads. As illustrated in Figure 1, the biphenyl group is represented by two CG C6 beads in 5P, by one CG C6 bead and two CG P3 beads in 6P, and by four CG P3 beads in 7P. Then, as for the parametrization of CG interaction potentials, we try to combine the aforementioned structure-based and thermodynamic quantities-based methods to reproduce multiproperties involving density, RDFs, and essential nematic features of 5CB at 300 K and 1 atm. Specifically, the nematic phase is considered as the key target for our parametrization process, as most applications of the 5CB are naturally in the nematic phase. In our proposed CG models, as there are at least 4 bead types and more than 10 different types of nonbonded interactions, and the nonbonded potential parametrization faces considerable difficulties. In this case it is advantageous to split the target molecule into small fragments as used by Peter for the liquid crystalline compound 8AB8,[44] and the nonbonded interaction potentials between CG beads can be determined such that the densities and structural properties (i.e., RDFs) of isotropic liquids of these fragmental molecules are reproduced. However, it is not clear whether these fragment-based potentials are equally well suited to reproduce the density and structural properties of the 5CB nematic phase at 300 K and 1 atm. Generally, the transferability of these fragment-derived CG potentials to the target molecules has to be tested with great care. Before reaching the most reliable model, we have to analyze and compare the performance of the proposed three different CG models with respect to reproducing the density, RDFs, and the nematic phase observed in atomistic simulations at 300 K and 1 atm. The results show that the 6P model is superior to the other two CG models. Then we use this model to study the nematic to isotropic (NI) phase transition temperature as well as the diffusion coefficients. A little beyond our expectation, these properties are also quantitatively reproduced. Consequently, a rational CG model and appropriate force field parameters are determined for the 5CB molecule. We also note that the CG simulation is at least 30 times faster than the corresponding atomistic simulation in achieving the same total simulation time, suggesting the advan tage of the CG model in the study of LC phase transitions that typically occur on larger systems at longer time scales.

This paper is organized as follows. In section 2 the CG models and interaction potentials are constructed for 5CB. Section 3 first illustrates the examination and comparison of results obtained with the three different models. Afterward the most reliable CG model is identified. Then the NI phase

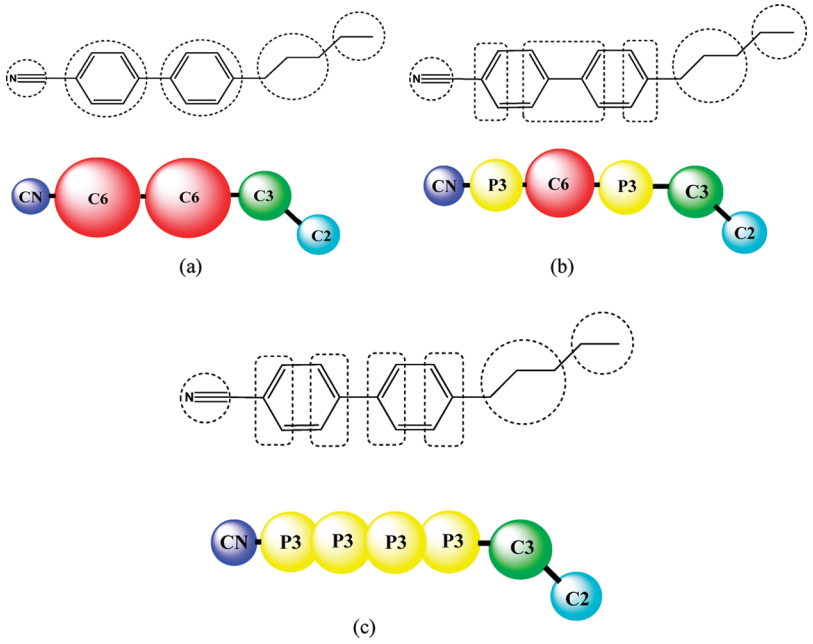

Figure 1. Three coarse-grained models (a) 5P, (b) 6P, and (c) 7P for the 5CB molecule. Circles in the atomistic 5CB representations in the upper panels correspond to CG beads in the coarse-grained representations in the lower panels.

transition and the diffusion coefficients are investigated by this model, which also serves as a check on the quality of this CG model. Finally, our main conclusions are given in section 4.

2. METHOD

To reproduce the phase behavior of the 5CB system accurately, a reasonable mapping scheme and an optimal force field are needed. In this section, we first illustrate how the coarse-grained models in close connections to the underlying atomistic representation are built, and then we devise an appropriate strategy to parametrize the bonded and nonbonded interactions.

2.1. Mapping Scheme. Since the mapping scheme is not unique, three feasible models have been constructed for the 5CB molecule in order to determine the optimal model through comparisons on their abilities in reproducing the specific properties under investigation. As shown in Figure 1, the 5P, 6P, and 7P models are named according to the number of CG particles, and the chief difference between them is in how the biphenyl segment is mapped. In spite of this difference, the mapping points are all taken as the group center of mass. The definition of the CG sites is given as follows. For the short aliphatic tail, a mapping of three and the remaining two methylene units respectively into one C3 bead and one C2 bead is chosen, similar to the current mapping of *n*-alkanes.[45] The cyano head is mapped into a single CG bead of type CN. For the remaining biphenyl segment, the 5p model assigns the benzene ring to a distinct spherical C6 bead so that the biphenyl segment is represented by two C6 particles, whereas in the 7P model, the benzene ring is partitioned into two P3 particles; consequently, the biphenyl segment is represented as four P3 particles. Very similar in spirit to our treating of the benzene ring in the 7P model, Lopez et al.[46] have constructed a similar CG representation of the benzene ring in the aryl amide molecule for probing membrane insertion activity of antimicrobial polymer. As illustrated in Figure 1, the 6P model is taken as an intermediate between 5P and 7P models, in which both C6 and P3 sites are used to build the biphenyl segment in 5CB. To preserve the shape of this biphenyl mesogenic unit in the CG construct, the moiety of each benzene ring is approximated using one P3 site, and the remainder of the biphenyl segment (that is, the remaining halves of two benzene rings) is modeled using a single C6 site such that the biphenyl segment is mapped into three CG beads of P3, C6, and P3 in the 6P model. As mentioned above, the mapping of the atomistic structure to the CG model is not unique; our choice of these three particular CG models is helpful to understand how the difference in mapping schemes affects the performance of the CG models with respect to reproducing structural and thermodynamical properties of the simulated system.

2.2. Potentials. Conventionally, the total potential energy U^{CG} is separated into bonded ($U_{Bonded}{}^{CG}$) and nonbonded ($U_{Non}{}^{CG}$) contributions

$$U^{CG} = \sum U^{CG}_{Bonded} + \sum U^{CG}_{Non} \quad (1)$$

Therefore, we can separately derive the bonded and nonbonded interaction potentials for the CG system in different ways.

2.2.1. Bonded Interaction. Intramolecular bonded interactions are derived such that the local conformational distributions of the molecules are reproduced in the CG MD simulations. The details are as follows. First, the CG conformational distributions, i.e., probability distributions of CG bond lengths ($P(r)$) and CG bond angles ($P(\theta)$), are generated from sampling the atomistic trajectory and then are inverted into tabulated CG interaction potentials by the Boltzmann inversion as below

$$U^{CG}(r, T) = -k_B T \ln(P^{CG}(r, T)/r^2) + C_r \quad (2)$$

$$U^{CG}(\theta, T) = -k_B T \ln(P^{CG}(\theta, T)/\sin(\theta)) + C_\theta \quad (3)$$

where C_r and C_θ are constants for setting the minima of the respective potentials to zero. Finally, the resulting tabulated

dx.doi.org/10.1021/jp210764h | J. Phys. Chem. B 2012, 116, 2075−2089

potentials are fitted into a set of simple efficient harmonic potentials by using the least-squares method

$$V_{bond} = 0.5*k_b*(l - l_0)^2 \quad (4)$$

$$V_{angle} = 0.5*k_a*(\theta - \theta_0)^2 \quad (5)$$

so the CG force constants K_a and K_b and the CG equilibrium bond length l_0 and angle θ_0 are obtained.

Usually, these CG conformational distributions are obtained either from an atomistic simulation of the bulk phase or from simulating an isolated molecule in vacuum atomistically. The former method has been successfully used by Shelley et al.[35] The latter has also been successfully used by Kremer's group,[23,44] but they also pointed out that deriving meaningful bonded potentials from an isolated molecule requires that the conformational samplings of the molecule in vacuum and in the bulk phase are similar to each other.[47] If the conditions are not satisfied, the resulting CG bonded potentials based on the conformational sampling of an isolated molecule would fail to reproduce the distribution functions of bond lengths and angles obtained from an atomistic simulation of the actually studied system. For our studied 5CB molecule, atomistic simulations showed that the conformation distributions of a single 5CB in vacuum differ substantially from those of 5CB molecules in the nematic phase at 300 K and 1 atm. Therefore, the CG bonded parameters derived from the two approaches are very different. For example, the length distribution profile for the bond between CG sites of C2 and C3 in the soft alkyl tail, which is calculated from an atomistic simulation of a single molecule in vacuum, has two peaks and the equilibrium length (if defined as the position of the highest peak) is about 0.22 nm, while the bond distribution profile determined from simulating the bulk nematic phase in atomistic resolution has a single peak and the resulting equilibrium length is 0.29 nm. Subsequent CG MD simulations with the bonded potentials from vacuum data indeed failed in appropriately reproducing the conformational distributions of the atomistic 5CB nematic phase. Thus, to properly model the local conformational statistics of the 5CB molecules in the nematic state, in this paper the bonded potentials are derived from an atomistic simulation of the bulk system rather than of an isolated molecule in vacuum. Note that for the rigid cyanobipheny fragment in the 5CB molecule, the derived force constants for CG bond stretching interactions between CN−C6 and C6−C6 in the 5P model, CN−P3, P3−C6, and C6−P3 in 6P, and CN−P3 and P3−P3 in the 7P model are significantly high. As a result, only a smaller time step, which is even comparable with those used in atomistic simulations, can be used in CG MD simulations. Otherwise, the molecule may be broken, and the whole system will be crashed. Peter[44] also pointed out such a problem in their CG simulations for 8AB8 liquid crystal. In order to use a longer time step while preserving the size of stiff cyanobipheny segment, we employ the Lincs method to constraint these rigid bond lengths. The final parameters for CG bond stretching interactions are listed in Table 1.

In addition, one essential molecular structure of the 5CB LC molecule is that it consists of a rigid cyanobipheny part and a soft alkyl part. After mapping, these two parts have already been reflected in our CG models. For example, in the 6P model, the bond bending potentials for two angles of C2−C3−P3 and C3−P3−C6 can control the flexibility of the alkyl tail, while those for the other two angles of P3−C6−P3 and C6−P3−CN can tune the stiffness of the rigid cyanobipheny segment. But,

Table 1. Force Field Parameters for Bond Stretching Interactions in the Three CG 5CB Models[a]

bond	R_0 (nm)	K_b (KJ/(mol × nm^2))	bond	R_0 (nm)	K_b (KJ/(mol × nm^2))
CN−C6 (5P)	0.335	fix	P3−C6 (6P)	0.308	fix
C6−C6 (5P)	0.424	fix	P3−C3 (6P, 7P)	0.29	20000
C6−C3 (5P)	0.3726	12247	P3−P3 (7P)	0.1-866	fix
CN−P3 (6P, 7P)	0.242	fix	C3−C2	0.29	9600

[a]Note that all specific bonds for any particular CG model are denoted.

during the parametrization of the bond angle bending potentials, we find that the potentials, for those two angles on the rigid part, which are directly derived by the Boltzmann inversion and fitting steps, are difficult to reproduce the target angle distributions. This failing is not surprising, as the degrees of freedom are reduced at the coarse-grained level. Thus, a further refinement of CG potentials is usually required in order to reproduce the target structural distributions in the CG MD.[25] It is also interesting to note that by using the harmonic function of eq 5 for bond bending potentials, the force constant K_b can be easily adjusted so that CG MD simulations could reproduce as closely as possible the angle distributions obtained from atomistically simulated system. Similar to the case of the 6P model, the force constants in the bond angle bending potentials for the triple beads in the rigid cyanobipheny segment of 5P and 7P models have to be refined to guarantee that the true angle distributions are reproduced in CG MD simulations. The full set of parameters for the bond bending interactions is listed in Table 2.

Table 2. Force Field Parameters for Bond Angle Interactions in the Three CG 5CB Models[a]

angle	K_a (kJ/(mol × rad^2))	deg
CN−C6−C6 (5P)	400	180
C6−C6−C3 (5P)	140	170
C6−C3−C2 (5P)	30	138
CN−P3−C6 (6P)	360	180
P3−C6−P3 (6P)	380	180
C6−P3−C3 (6P)	95	163
P3−C3−C2 (6P, 7P)	50	143
CN−P3−P3 (7P)	340	180
P3−P3−P3 (7P)	360	180
P3−P3−C3 (7P)	136.8	157.5

[a]Note that all specific angles for any particular CG model are denoted.

The resulting CG angle distributions obtained from CG MD simulations with these bonded parameters, as listed in Table 1 and Table 2, turn out to approximately reproduce the true conformational distributions of the atomistic 5CB in the nematic phase. An example for the typical CG angle distributions can be seen in Figure 2 for the case of the 6P model, and for comparison the corresponding data from atomistic simulations are also plotted. It appears that the angle distributions of CG and atomistic simulations are matched to each other within a certain level of accuracy. The peak positions of the distribution functions from atomistic and CG simulations almost coincide except for the angle CN−P3−C6 shown in Figure 2d, although such a deviation is still acceptable to some

dx.doi.org/10.1021/jp210764h | J. Phys. Chem. B 2012, 116, 2075−2089

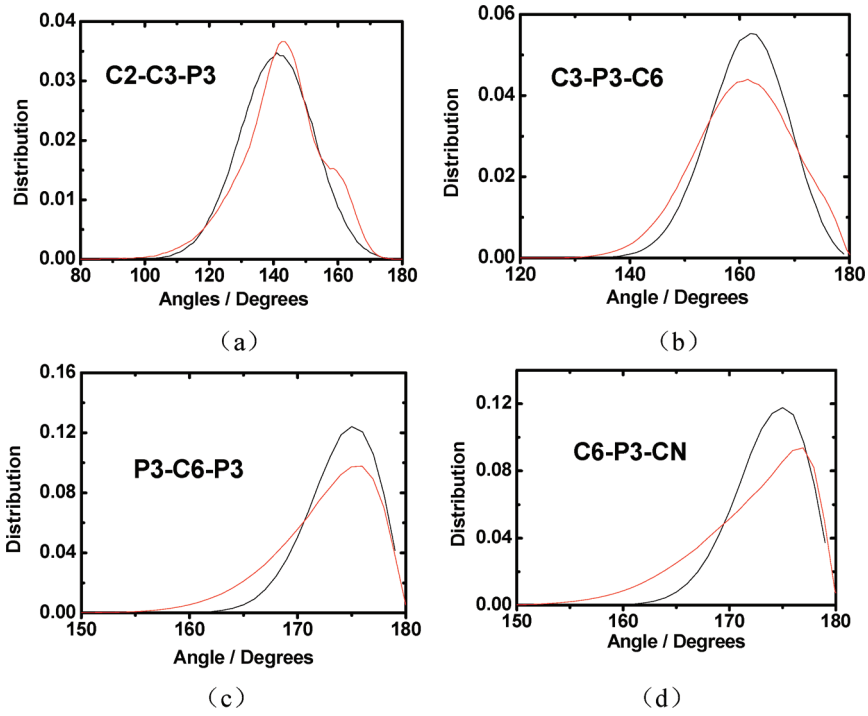

Figure 2. Comparison of the angle distributions between the atomistic (black line) simulations of the 5CB nematic phase and the corresponding CG (red line) simulations of the 6P model.

extent. This deviation may come from the choice of functional form for the bond bending potential, because a harmonic potential, which is symmetrical, is used to fit an unsymmetrical numerical potential curves of angles, even if the force constant K_b is refined later on. Therefore, a different choice of functional form may improve the situation.

It should be noted that in the present ansatz the refinement of some angle parameters (as addressed above) and the subsequent optimization of some nonbonded parameters (as will be shown in section 2.2.2, undertaking this process is due to the poor applicability of these nonbonded parameters derived from fragment-based method) are based on the CG MD simulations of the 5CB bulk phase; consequently, the present reparameterization of these CG angle interactions will be affected by the use of the nonbonded parameters, and the later reparameterization process of these CG nonbonded interactions will be affected by the selection of the bonded parameters. Such interdependence not only means that these parametrization processes are not as rigorously separated but also indicates that it is not possible to optimize these bonded and nonbonded parameters simultaneously. It is advisible to follow a particular sequence to optimize them. First, a series of CG MD simulations are performed with the previously determined bonded parameters, among which the CG angle parameters for the rigid cyanobiphenyl segment are unrefined. Meanwhile, one adjusts the nonbonded parameters, which are selected to be optimized, to reproduce the density of the 5CB nematic phase in CG MD. Since unlike other CG target quantities, such as the RDFs and essential nematic features of 5CB, the thermodynamic quantity density is more sensitive to the excluded volume of the CG beads than to the local conformations, we found that the density is reproduced within a small deviation of 2% by using the unrefined bonded parameters. Then, additional CGMD simulations are performed with the fixed nonbonded parameters, some of which are directly derived from the fragment-based method, and the rest are obtained through the above optimization process. Simultaneously, the angle parameters, which are chosen to be refined, are tuned in order to closely reproduce the angle distributions obtained from atomistic MD. By doing so, the angle parameters, which can better reproduce the angle distributions of the atomistic 5CB nematic phase and still keep the density properly matched to the target value, are developed. It should be mentioned that for the latter optimization process of nonbonded parameters a series of CG MD simulations are performed by applying the above optimized bonded parameters. Then the nonbonded parameters, which are chosen to be optimized, are determined in a systematic way with an aim to match a set of thermodynamic and structural quantities (the density, RDFs, and the nematic phase at 300 K and 1 atm) as we will show in section 2.2.2. By doing so, the nonbonded parameters, which can better reproduce thermodynamic and structural quantities without disrupting the local conformational properties, are determined. Indeed, the CG force field parametrization is a crucial step, which determines the predicting power of CG models, and devising a careful guideline is thus important for reaching reliable interaction parameters.

2.2.2. Nonbonded Interaction. As for the CG nonbonded interaction potentials, two principal forms of potential functions[44] are usually used. One is the analytical potential such as Lennard-Jones (LJ) form potential (e.g., 12−6, 9−6, or 7−6) and Morse potential. Another is the numerically derived tabulated potential. Generally, the choice of functional forms is dependent on the system under study as well as the intended use of the CG model.[26] Because the CG particles are rather large and soft, in our simulation, a common functional form of soft LJ 9−6 potential is selected for nonbonded interactions

$$U_{9-6}(r) = \frac{27}{4}\varepsilon\left(\left(\frac{\sigma}{r}\right)^9 - \left(\frac{\sigma}{r}\right)^6\right) \quad (6)$$

dx.doi.org/10.1021/jp210764h | J. Phys. Chem. B 2012, 116, 2075−2089

Table 3. Liquid Systems Used for Parameterizing the Nonbonded LJ 9−6 Potentials (Bead Types Labeled According to Figure 1) and Comparisons of Densities between Experiments and CG Simulations as Well as Deviations of Radial Distribution Functions for the CG Sites between CG and Atomistic Simulations

systems	types of CG particles	densities from experiments[49,50] (g/cm^3)	densities derived from CG simulations (g/cm^3)	deviations of densities	RDF deviations ($\times 10^{-3}$)
dodecane	C2	0.7487	0.765	2.1%	4.1
dodecane	C3	0.7487	0.754	0.7%	12.8
benzene	P3	0.8740	0.865	1.0%	21.1
benzene	C6	0.8740	0.870	0.4%	52.1
butyronitrile	CN	0.7800	0.784	0.5%	1.3
butyronitrile	C3	0.7800	0.784	0.5%	5.0

where the parameters ε and σ are the minimum energy and the distance at $U = 0$, respectively. The standard Lorentz−Berthelot[48] mixing rules of $\varepsilon_{ij} = (\varepsilon_i \times \varepsilon_j)^{1/2}$ and $\sigma_{ij} = (\sigma_i + \sigma_j)/2$ were used for calculating the LJ parameters between different types of CG beads.

As mentioned in the Introduction, we choose a new strategy which combines structure-based and thermodynamic quantities-based methods and thus use the density and radial distribution functions as well as nematic phase of 5CB systems as targets for the parametrization of the nonbonded potentials for CG simulations. Since there are at least four bead types in our proposed CG models, we have to adopt the fragment-based approach and split the target molecule into small fragments. At this stage, the first priority is to parametrize the nonbonded interaction potentials between CG beads of the same type based on the structures and densities of isotropic liquids of these fragment molecules. According to the fragment molecules, a series of atomistic MD simulations for several isotropic liquids are carried out to fix the nonbonded interaction parameters in a systematic way as described below.

First of all, the isotropic liquids used to parametrize particular bead types are selected. As listed in Table 3, in the present work liquid dodecane is used in the parametrization process for beads C3 and C2, liquid benzene for C6 and P3, and liquid butyronitrile for CN. We then take liquid dodecane as an example to illustrate the subsequent steps for deriving the nonbonded LJ 9−6 potential parameters σ and ε. In this case, an atomistic simulation of isotropic dodecane liquid has been performed to get density and structural data (i.e., RDFs), which can be used as targets to be reproduced by the CG models. According to the structural feature of the dodecane molecule, each dodecane molecule can be mapped into four CG beads (type C3) or six CG beads (type C2). The bonded interaction potentials of C3 or C2 beads can be determined using the approach introduced in section 2.2.1. The nonbonded interaction potentials between C3−C3 or C2−C2 pairs can be derived by tuning the two parameters σ and ε to reproduce the target density and RDFs. However, the target density is often reproduced by several sets of LJ parameters within a small density deviation of 2% due to a simultaneous parametrization of the two parameters ε and σ. In this case, the RDF is used as an additional criterion to judge which set of LJ parameters is a better representative for the particular bead types. The deviation of the RDFs between atomistic and CG simulations has been calculated through the equation as defined below

$$\Delta g(r) = \sum_{1}^{N} e^{-r_i}[g_{cg}(r_i) - g_{target}(r_i)]^2 \Delta r \quad (7)$$

Here $g_{target}(r_i)$ and $g_{cg}(r_i)$ are the target RDF and the actual RDF calculated from atomistic and CG simulations, respectively. Generally, if the deviation is of the order of 10^{-3}, we will consider that the target RDF has been closely reproduced. Hence the LJ parameters with the smallest deviation of RDFs between atomistic and CG simulations are chosen for the C3−C3 and C2−C2 pairs. Again, following the above parametrization procedure, the LJ parameters of CN−CN, C6−C6, and P3−P3 pairs are obtained from liquid butyronitrile and benzene systems, respectively. We should note that the CG model of the butyronitrile molecule is represented by a CN site and a C3 site, and thus the LJ parameters of the CN−CN pair are determined by adopting the LJ parameters of the C3−C3 pair to the above derived values based on liquid dodecane. The mixed interaction between CN and C3 beads is approximated by the standard Lorentz−Berthelot mixing rules as mentioned above. The full set of LJ parameters for the pair interactions between the same CG beads is reported in Table 4. The relevant CG bonded interaction parameters for the dodecane, benzene, and butyronitrile molecules are listed in the Tables S1 and S2 in the Supporting Information.

Table 4. LJ Parameters for the Pair Interactions between the Same C Beads Based on the Isotropic Liquids of Fragment Molecules

type	σ (nm)	ε (kJ × mol^{-1})
C3 (dodecane)	0.47	1.8963
C2 (dodecane)	0.43	1.0667
C6 (benzene)	0.50	3.6740
P3 (benzene)	0.46	1.4220
CN (butyronitrile)	0.36	1.8963

Additionally, the densities of the three (dodecane, butyronitrile, and benzene) liquids obtained from CG MD simulations with these fragment-based LJ parameters are also listed in Table 3. We can see that all densities are reproduced very well, and the largest deviation with a value around 2.1% comes from liquid dodecane when the dodecane molecule is coarse-grained with C2 beads. At the same time, the RDFs of CG sites of C3−C3, C2−C2, CN-CN, C6−C6, and P3−P3 obtained from both atomistic and CG simulations on the corresponding isotropic liquids are calculated. As shown in Figure 3, all the RDF peaks of the atomistic liquids are almost reproduced, and most of the deviations of RDFs (reported in Table 3) are at the level of about 10^{-3}. Among them, liquid benzene, when one benzene molecule is mapped into one spherical C6 bead or two spherical P3 beads, displays a relatively higher first peak with the RDF deviation of about 10^{-2}, suggesting that although a softer LJ 9−6 potential (compared to LJ 12−6) has been used

dx.doi.org/10.1021/jp210764h | J. Phys. Chem. B 2012, 116, 2075−2089

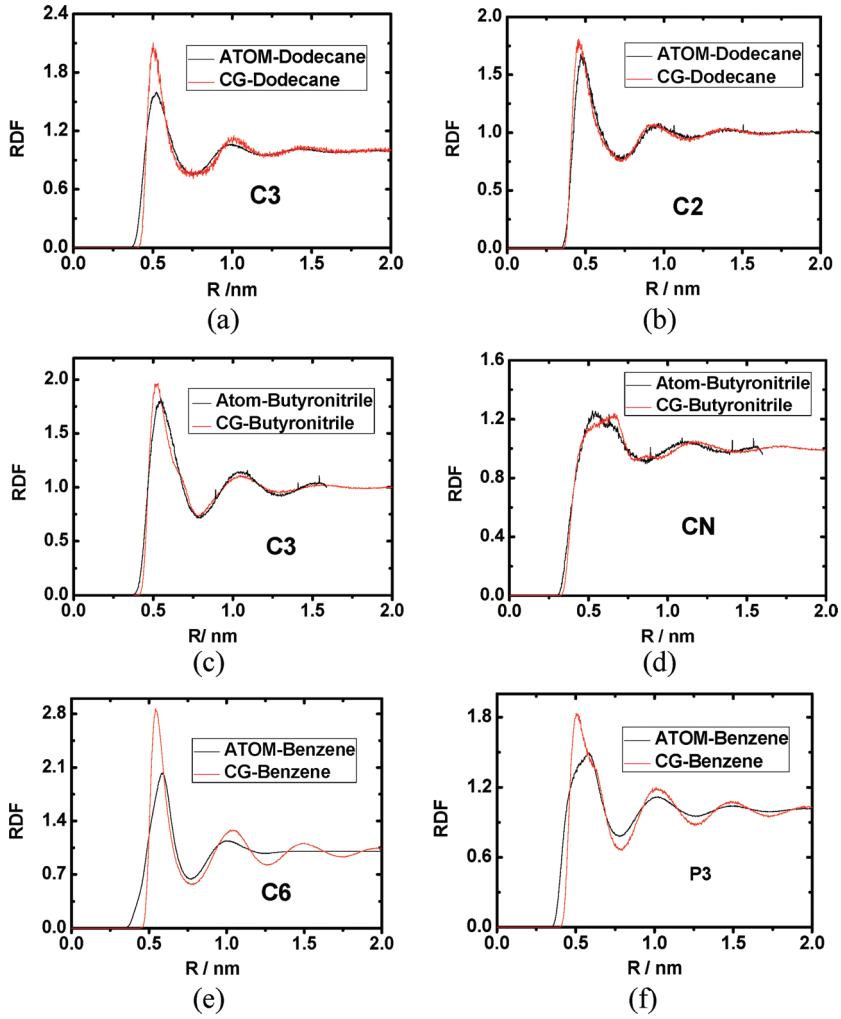

Figure 3. Radial distribution functions of (a) C3−C3 and (b) C2−C2 sites in liquid dodecane, of (c) C3−C3 and (d) CN−CN sites in liquid butyronitrile, and of (e) C6−C6 and (f) P3−P3 sites in liquid benzene obtained from CG and atomistic simulations.

Table 5. Liquid Systems Used for Testing the Transferability of the LJ Parameters Derived from Fragment Methods and Comparison of Densities between CG Simulations and Experiment as Well as Deviations of RDFs between the CG and Atomistic Simulations

systems	types of CG particles	densities of experiments[49,50] (g/cm^3)	densities of CG simulations (g/cm^3)	deviation of density	RDF deviation ($\times 10^{-3}$)
hexane	C2	0.6548	0.645	1.4%	1.2
hexane	C3	0.6548	0.650	0.7%	7.8
octadecane	C2	0.7800	0.792	1.5%	5.9
octadecane	C3	0.7800	0.791	1.4%	14.9
biphenyl	C6	1.0400	0.963	7.4%	32.5
biphenyl	P3	1.0400	1.067	2.4%	43.6
hexylbiphenyl	C6	0.9880	0.950	3.8%	63.2
hexylbiphenyl	P3	0.9880	1.046	5.9%	132.1
benzonitrile	CN	1.0100	0.985	2.4%	16.1
benzonitrile	P3	1.0100	0.985	2.4%	11.0

between the CG beads, discrepancies at the level of local packing of benzene molecules between atomistic and coarse-grained models cannot be removed. Nevertheless, the density of atomistic liquid benzene has been reproduced well, so the LJ nonbonded parameters for CG beads of C6 and P3 are still acceptable for liquid benzene to some extent.

Then, we further test the transferability of the above-derived nonbonded parameters, as the parametrization from fragment molecules is expected to have the possibility of reusing certain nonbonded interaction potentials for recurring building blocks.[32] As reported in Table 5, liquid octadecane and liquid hexane have been used to test the transferability of the nonbonded parameters for C3−C3 and C2−C2 pairs, liquid biphenyl and liquid hexylbiphenyl for P3−P3 and C6−C6 pairs, and liquid benzonitrile for CN−CN and P3−P3 pairs. A series of CG MD simulations have been performed on the CG models of

dx.doi.org/10.1021/jp210764h | J. Phys. Chem. B 2012, 116, 2075−2089

these testing systems with the just determined nonbonded potentials, whereas the CG bonded interactions are derived from sampling the corresponding distributions of the atomistic simulation of the same molecular system using the approach introduced in section 2.2.1. All the resulting densities for the CG models of testing systems and the deviation of RDFs between the CG and atomistic simulations for the pairs of the same CG beads of C2, C3, CN, P3, and C6 are listed in Table 5. The RDF profiles for the C2−C2, C3−C3, CN−CN, P3−P3, and C6−C6 pairs from the CG and atomistic simulations on the testing systems are shown in Figure S1 in the Supporting Information. It is found that the resulting densities and RDFs from the CG simulated two alky systems are in good agreement with the experimental values and their atomistic counterparts, respectively, suggesting that C3−C3 and C2−C2 nonbonded parameters can be extrapolated to the alky tail of the 5CB molecule. For the liquid biphenyl and the liquid hexylbiphenyl, as reported in Table5, the density deviation is in the range from 2.4% to 7.4% and RDFs deviate more remarkably from those obtained from the corresponding atomistic simulations, indicating that C6−C6 and P3−P3 nonbonded parameters based on liquid benzene are not applicable to reproduce the density and structure of these two test systems. It is probably due to the difference in the packing of phenyl rings in the liquid benzene and in the biphenyl or hexylbiphenyl systems. Given this, the current nonbonded parameters of P3−P3 and C6−C6 are likely nontransferable to the rigid part (i.e., biphenyl) of the LC 5CB molecule, and they need to be reparameterized. Finally, when the test molecule benzonitrile is mapped into one CN bead and two P3 beads, as shown in Table 5, the density deviation is about 2.4% and the RDF deviations for the P3−P3 and the CN−CN pairs are about 11×10^{-3} and 16×10^{-3}, respectively, suggesting that unlike the above two test systems of liquid biphenyl and liquid hexylbiphenyl the fragment-based nonbonded parameters of P3 and CN are better suited to reproduce the density and structure of the liquid benzonitrile. In short, although the resultant nonbonded parameters based on liquid benzene are less transferable, the procedure to derive CG potentials from isotropic liquids of fragmental molecules does still in part make the CG parameters transferable to different systems with different compositions.

We note that the current C6 and P3 parameters are expected to be problematic if applied in CG MD simulations on the 5CB system. Indeed, when the fragment-based nonbonded parameters, as listed in Table 4, were used for the 5CB system, our CG MD simulations show that both density and RDFs deviate notably from the target quantities, which has further led to the incorrect phase behavior. Although these simulations were performed initially with unrefined bonded potentials as mentioned in section 2.2.1, which may affect the resulting properties, the nontransferability of the nonbonded parameters of C6−C6 and P3−P3 requires us to reparameterize them to quantitatively reproduce the target density first while fixing the rest of the nonbonded parameters to the fragment-based values in order to maintain transferability of our CG models at least to some extent. Also as addressed in section 2.2.1, the reparameterization process of the C6−C6 and P3−P3 potentials is not so rigorously separated from the reoptimization of CG angle interactions. By adjusting manually the nonbonded interaction parameters σ and ε for C6−C6 and P3−P3 pairs, we found that the target density is reproduced within a small deviation of 2% by using the unrefined bonded parameters. Then the CG angle potential parameters are refined with the introduction of just optimized C6−C6 and P3−P3 parameters. Afterward the reasonable CG angle potentials are derived, which can not only better reproduce the angle distributions of the atomistic 5CB nematic phase but also keep the density properly matched to the target value. Finally, as we will see below, more efforts are made to optimize the LJ parameters, namely the contact distance σ and the well depth ε, for C6−C6 and P3−P3 pairs, while applying the previously refined bonded parameters in order to reproduce the target density and RDFs as well as the nematic phase of 5CB systems at 300 K and 1 atm.

Unlike 5P and 7P models, the 6P model contains both P3 and C6 beads; thus, the procedure to optimize their LJ parameters is more complicated. For computational convenience, we take a strategy to separately treat the P3 and C6 beads. First, we start the optimization of P3−P3 LJ parameters by keeping C6−C6 LJ interactions fixed at the previously determined parameters which approximately reproduced the density of 5CB. In this case, since the initial LJ parameters can reproduce experimental densities, the P3−P3 pair distribution function obtained from the atomistically simulated 5CB system is used to determine the LJ parameters for P3−P3. With this choice, we adjust manually the two parameters ε and σ to closely reproduce the target structural distribution between the P3 beads. We then fix ε and σ values for the P3−P3 pair, as reported in Table 6, such that the CG distribution function correctly describes the position of the peaks, especially of the first one, and the resulting density deviation is maintained smaller than 2%.

Table 6. Final Nonbonded LJ Interaction Parameters for Coarse-Grained Simulations of 5CB Using the 6P Model

type	σ (nm)	ε (kJ × mol^{-1})
C3	0.470	1.8963
C2	0.430	1.0667
CN	0.360	1.8963
C6 (5CB−6P)	0.545	3.5556
P3 (5CB−6P)	0.460	1.4815

Second, the LJ parameters for the C6−C6 interaction are optimized in a systematic way in order to properly match a set of quantities such as bulk density, radial distribution functions, and nematic phase of 5CB systems at 300 K and 1 atm, which are either obtained from experiments or calculated from the atomistic model. In this case, the C6−C6 LJ parameters are refined while applying the previously optimized P3−P3 LJ parameters. Since the target bulk density is taken into account in the previous parametrization, the first option is to adjust the LJ parameters to reproduce the specific thermodynamic phase, that is, nematic phase. The reason we used nematic phase as the first priority target for the reparameterization process is that most applications of 5CB are naturally in the nematic phase and the reproduction of the 5CB nematic phases is essential. Meanwhile, this reparametrization will directly build the specified nematic phase structure into the C6−C6 LJ potential. The further optimization of C6−C6 LJ parameters is made to obtain as close a match as possible between the structural distributions from a simulation of the CG model and from a simulation of the atomistic model. However, certain discrepancies at the level of local packing between the atomistic and the CG description can be expected. The reason for this is that coarse graining the groups of atoms into spherical CG beads with radically symmetric CG potentials often bears the problem that the link to the underlying structure and the reproduction of local structural properties (i.e., pair distributions) may become weak.

In particular, the discrepancy may become even stronger for the C6 bead, which represents the halves of two benzene rings in the rigid biphenyl group in which those atoms in the respective half are in the same plane. Additionally, we should mention that the simplification of mixed interactions between different types of CG beads according to the Lorentz−Berthelot rule would also affect the quantitative reproduction of local structural properties. This degree of discrepancy, however, is not a critical issue as long as our main concern is in the phase behavior of the 5CB liquid crystal system (i.e., the nematic to isotropic phase transition (NI) temperature). In fact, as we will show in the next section, the reparametrization of the C6−C6 LJ parameters has proved to be remarkably successful, since there is consistency in the NI transition temperature, neighboring molecular pair arrangements, and diffusion properties among these CG and atomistic simulations as well as experimental measurements. All the final nonbonded interaction parameters for the identical CG bead pairs in the 6P model are listed in Table 6.

However, CG MD studies show that the 5P model using the just optimized C6−C6 LJ parameters is not well suited to reproduce the thermodynamic properties of the 5CB system at 300 K and 1 atm. In this case the 5CB nematic phase becomes unstable. It is not surprising that the derived C6−C6 LJ parameters are nontransferable, since unlike in the 6P model, the C6 bead in the 5P model, as illustrated in Figure 1, represents a benzene ring, and the resultant C6−C6 LJ parameters for the 6P model are specific to the packing of the corresponding groups of atoms in the sampled atomistic MD system. As a consequence, the C6−C6 LJ parameters have to be modified for use in the 5P model. Similarly, greater emphasis is placed on the reproduction of the nematic phase of 5CB systems at 300 K and 1 atm, and a combination of experimental density and the structure data (i.e., RDF for the C6−C6 pair) from the atomistic simulations is also used for parameter fitting. It should be mentioned that even if several sets of the LJ parameters are chosen such that the resulting density is comparable with the experimental value (the deviation is within ±2%) and the resulting positions of the RDF peaks (especially of the first one) are also comparable with those of atomistic simulations, the subsequent CG MD simulations cannot exactly reproduce the nematic phase at 300 K and 1 atm. Further optimizing the performance of the 5P model with respect to reproducing the nematic phase does not fully correct this problem. The limitation of the current 5P model in describing the nematic phase points out that the simplification of representing *a benzene ring in which all atoms are in the same plane* as a spherical CG bead might not correctly reproduce the packing of phenyl rings in the 5CB nematic phase.

Meanwhile, it can be seen that the 7P model with the P3−P3 LJ parameters determined from the 6P model is not suited to reproduce the structure of the 5CB system at 300 Kand 1 atm. Therefore, the expected 5CB nematic phase becomes unstable, consistent with the above case of directly using the C6−C6 LJ parameters specific for the 6P model in the 5P model. The loss of transferability is not a desirable situation. However, as mentioned before, the resultant P3−P3 LJ parameters are derived according to the atomistic RDFs and reflect the specific chemical interactions between the corresponding groups of atoms in the benzene ring. Since the parametrization process incorporates detailed structural information at the level of the center of mass of the CG beads into the effective pair interaction, the differences in the CG mapping schemes between the 6P and 7P models (i.e., the rigid biphenyl group is represented respectively as P3−C6−P3 in 6P and as P3−P3−P3−P3 in 7P) may limit the range of applicability of the P3−P3 LJ parameters. Therefore, the P3−P3 LJ parameters have to be reparameterized by following the same procedure as used previously for the C6−C6 LJ parameters in the 5P model. Analogous to the 5P model, the 7P model cannot reproduce the 5CB nematic phase at 300 K and 1 atm. Again, the representation of a benzene ring in which all atoms are in the same plane as two spherical CG beads is not suited to model the packing of phenyl rings observed in atomistic simulations of the 5CB nematic phase.

Obviously, differences in the CG mapping schemes have significant consequences for the results of the CG simulations, and the 6P model is superior to its 5P and 7P counterparts. It is well-known that to link the CG results to the real chemical system one needs to appropriately devise the CG model and interaction potentials.[25] Since the mapping of the atomistic structure to the CG model is not unique but at the same time very crucial in terms of both efficiency and predicting power,[39] testing on various possible options to optimize the performance of the CG model with respect to reproducing the target properties is critically important. So far, few studies have been pursued with the aim to design mapping schemes and learn something about their capacities. Thus the systematic formal procedure for the CG mapping is currently unavailable. We hope our work will inspire further studies toward CG model development.

Besides, our step-by-step approach to construct the CG force field is significantly different from previous methods. We combine the aforementioned structure-based and thermodynamic quantities-based methods for the parametrization of CG interaction potentials and attempt to use several fragment molecular systems to derive the CG nonbonded interaction parameters in order to maintain the transferability of our CG models to some extent. Lastly, we fix the optimal nonbonded LJ parameters between the identical CG bead pairs such that the results from CG simulations not only correctly reproduce the experimental density and the nematic LC state at 300 K and 1 atm but also reasonably approximate the local structural properties (i.e., RDFs) calculated from the atomistic model. Note that currently there is considerable interest in how to derive CG potentials that are both thermodynamically as well as structurally consistent with the underlying atomic description.[39] However, the manual process of selecting a good LJ parameter set is drawback of our approach.

2.3. Simulation Details. A series of MD simulations of different systems including 5CB, its fragment molecules, and the liquids used for testing the transferability of the FF parameters have been carried out at the atomistic as well as the CG levels.

2.3.1. Atomistic MD. All the atomistic simulations were performed on GROMACS software[51] with reoptimized force field parameters,[18] which are based on TraPPE-UA force field,[52−56] except for the butyronitrile system using the original TraPPE-UA force field.[55] The NTP ensemble was taken for all systems, and the Nose−Hoover thermostat[57,58] and Parrinello−Rahman barostat[59] were used to maintain temperature and pressure at 300 K and l atm, respectively. The corresponding coupling time constants were 0.5 ps for temperature and 1.0 ps for pressure. All the bond lengths were constrained with the Lincs algorithm, and a time step of 1 fs was employed. A twin-range cutoff method with a short cutoff of 1.2 nm and a long one of 1.5 nm was used for the nonbonded van der Waals and electrostatic interactions.

The long-range electrostatic interactions were evaluated with the PME (particle-mesh Ewald) method.

2.3.2. CG MD. All CG MD runs were performed with the program GROMACS 4.05[51] in the NTP ensemble at 1 atm and several different temperatures. A Nose−Hoover thermostat[57] was employed to keep the temperature constant with a coupling time of 0.1 ps, while the Parrinello−Rahman barostat[59] was used to control the pressure with a coupling time of 1.0 ps. Nonbonded interactions were truncated by the twin-range cutoff method with a short cutoff of 1.2 nm and a long one of 1.5 nm. During all runs for 5CB, the rigid bond lengths were kept fixed at their equilibrium value with the Lincs algorithm and a time step of 10 fs was employed. In this work, all the runs were performed on a system of N = 2048 5CB molecules with periodic boundary conditions. For each temperature, the equilibration of these runs was accessed by monitoring total energies, densities (ρ), and orientational order parameters (P_2). Because of the long time scale involved, particularly near the NI transition temperature, the simulations at each temperature were run sufficiently long to reach equilibration, and then additional production runs of at least 200 ns were used in order to yield reliable results.

To monitor the evolution of the system, the internal energy, the bulk density, and the orientational order parameter P_2 have been calculated. P_2 is defined as the largest eigenvalue of the Saupe ordering matrix $\mathbf{Q}$[60]

$$Q_{ab} = \left\langle \frac{3}{2}u_a u_b - \frac{1}{2}\delta_{ab} \right\rangle \tag{8}$$

where the mean value $\langle ... \rangle$ is obtained by averaging on all the molecules, and u_a ($a = x, y, z$) is the vector of molecular long axis defined on the basis of the CN−C6 vector for the 5P and 6P models and of the CN−P3 vector for the 7P model (Figure 1). The director n is identified as the eigenvector corresponding to P_2. The value of P_2 will be close to 0 in the isotropic phase but tends to 1 in a highly orientational ordered phase. In our simulation, we could distinguish the isotropic phase from the nematic phase by looking at this order parameter. Additionally, because of the finite system size, the value of P_2 in the isotropic phase is small but nonzero.

In order to fully characterize the phase, the detailed structures of the LC phases were also investigated by the various distribution functions. One quantity is the orientational pair correlation function, which measures the decay of intermolecular angular correlations as a function of their distance and can thus be used to quantify the orientational order of a phase. Two orientational correlation functions are computed as

$$g_1(r) = \langle \cos \theta_{ij}(r) \rangle \tag{9}$$

$$g_2(r) = \left\langle \frac{3}{2}(\cos \theta_{ij}(r))^2 - \frac{1}{2} \right\rangle \tag{10}$$

where $\theta_{ij}(r)$ is the angle between the long axes (as defined above) of two molecules i and j, and r is the distance between the reference sites on two different molecules, i.e., the center of mass of cyano group. It is worth mentioning that $g_1(r)$ can give information on the local polar ordering, while $g_2(r)$ becomes long-ranged in the NI transition and its ultimate value at large r tends to $\langle P_2 \rangle^2$.

The radial distribution function (RDF) from atomistic simulations is used as one of the target quantities to derive the CG interaction potentials. We calculate the RDF between a site k in molecule i and a site m in molecule j as

$$g(r) = \frac{1}{4\pi r^2 \rho_N} \left\langle \delta(|r_i^k - r_m^j| - r) \right\rangle \tag{11}$$

where the mean value $\langle ... \rangle$ is a double average over all molecules and all time origins, and ρ_N is the number density.

To further explore the reliability of our FF, we also investigate one important aspect of the dynamical behavior, namely, the translation diffusion. The diffusion coefficients D_α are computed from

$$D_\alpha = \lim_{t\to\infty}\left(\frac{1}{2t}\right)\left\langle \sum_{j=1}^{N} [R_j^\alpha(t) - R_j^\alpha(0)]^2 \right\rangle \tag{12}$$

where $\alpha = x, y, z$. R_j^α is the position of the center of mass of molecule j projected onto the reference axis.

3. RESULTS AND DISCUSSION

The main purpose of the present work is to build an appropriate CG model for the liquid crystalline 5CB molecule that enables an efficient study of its phase behavior. Since the mapping scheme is not unique but very crucial in terms of both efficiency and predicting power, three different but closely related CG models, i.e., 5P, 6P, and 7P, are proposed. To construct the optimal CG force field, we combine the aforementioned structure-based and thermodynamic quantities-based methods and devise a careful guideline to parametrize the CG interaction potentials in a systematic way. By comparing to what extent the target properties can be reproduced by these three different CG models, the most reliable CG model is identified. Finally, the quality of this CG model is further confirmed by investigating another two important properties, the NI transition temperature and the diffusion coefficient.

3.1. Comparison of 5P, 6P, and 7P Models. As mentioned above, the most suitable model should reproduce the density, RDFs, and especially the nematic phase of 5CB at 300 K and 1 atm. We find that for the 5P model, through adjusting the LJ parameters of the C6−C6 pair to proper values such that the resulting density is comparable with the experimental value (the overestimation is within ±2%) and at the same time the resulting positions of the first peaks of the RDFs can also be comparable with those of atomistic data (shown in Figure S2 in the Supporting Information), a stable nematic phase has not been shown. Similar phenomena have been found for the 7P model.

As to the 6P model, which can be considered as a compromise between 5P and 7P models, the resulting density is about 1.003 g/cm^3 at 300 K and 1 atm and is very close to the experimental value[13] of 1.02 g/cm^3, wherein the deviation is less than 2%. The comparison of RDFs between atomistic and CG simulations has also been executed, and the results are shown in Figure 4.

The positions of the peaks, especially of the first one, from CG simulations for all types of CG beads except for C6 closely match those from atomistic simulations. It is worth noting that although the electrostatic interactions which are important for atomistic simulations are ignored in our CG simulations, the position of the first peak of RDFs for the CN−CN pair still matches each other. A relatively large deviation occurs for the

dx.doi.org/10.1021/jp210764h | J. Phys. Chem. B 2012, 116, 2075−2089

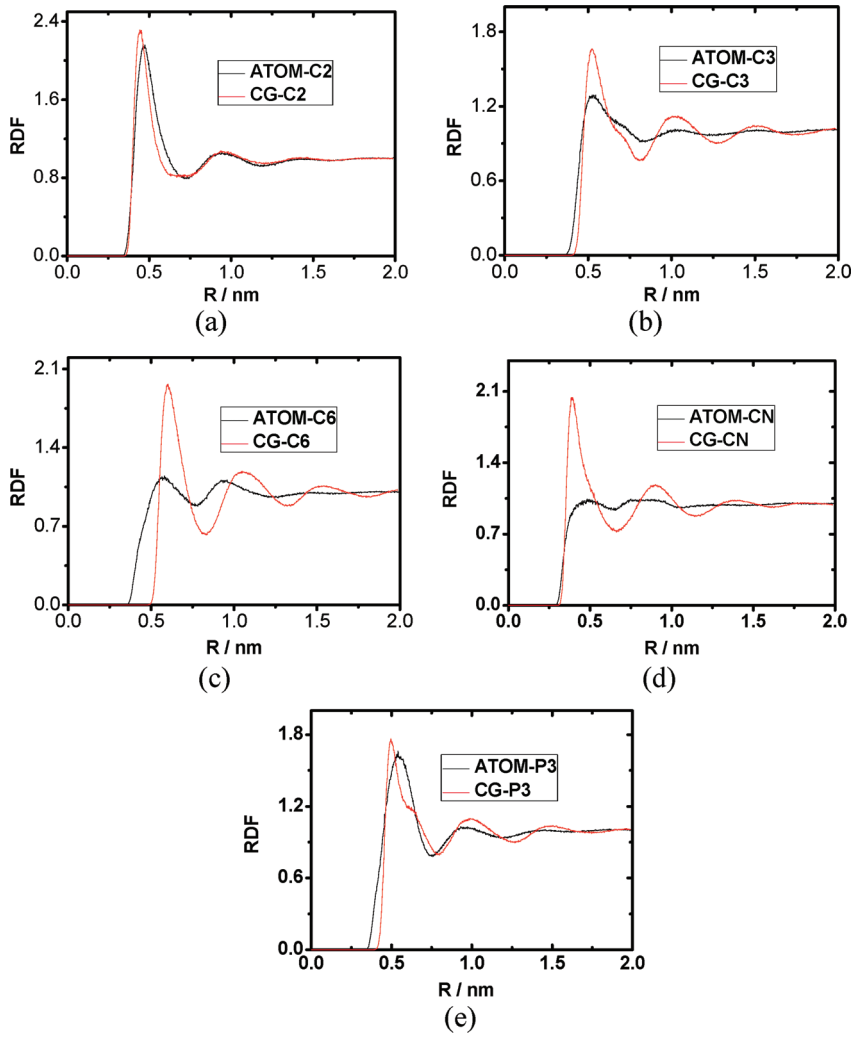

Figure 4. Target RDFs between C2, C3, CN, P3, and C6 beads in the atomistically simulated 5CB system at 300 K and 1 atm and the corresponding results from the CG simulations on the 6P model.

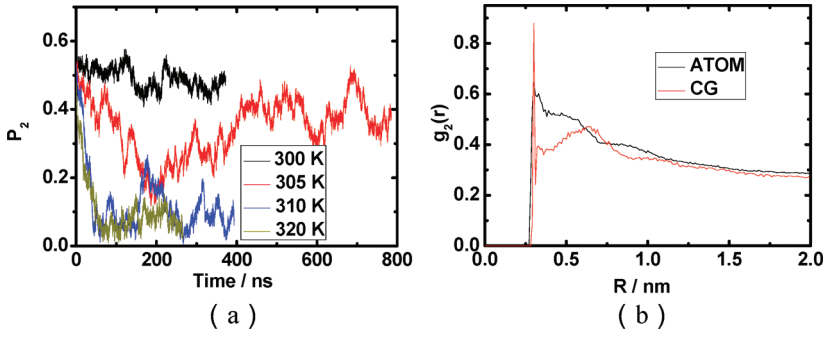

Figure 5. (a) Order parameters as a function of time at several temperatures for CG simulations of the 6P model system. (b) Orientational correlation functions $g_2(r)$ as a function of the distance between the centers of mass of the CN groups from atomistic MD or between CN beads from CG MD (with 6P model) simulations at 300 K.

C6 bead, whose first peaks are located at 0.60 and 0.57 nm for CG and atomistic simulations, respectively. As addressed in section 2, this discrepancy at the level of local packing between the atomistic and the CG description can be expected. Nevertheless, the nematic phase is reproduced well. As illustrated in Figure 5a, at 300 K, the average value of P_2 is 0.48, very close to the experimental value of 0.54,[12] and the fluctuation of P_2 is quite small, indicating the system forms a stable nematic phase at 300 K. Furthermore, as presented in Figure 5b, the values of the orientational correlation function $g_2(r)$ from the CG and atomistic simulations decay together to a similar value of $\langle P_2 \rangle^2$, providing more evidence for the stable nematic phase at 300 K.

To characterize the arrangement of 5CB molecules in the nematic phase, we have calculated the orientational correlation function $g_1(r)$. Interestingly, as seen from Figure 6, the $g_1(r)$ from the CG simulation shows a large negative value at short

dx.doi.org/10.1021/jp210764h | J. Phys. Chem. B 2012, 116, 2075–2089

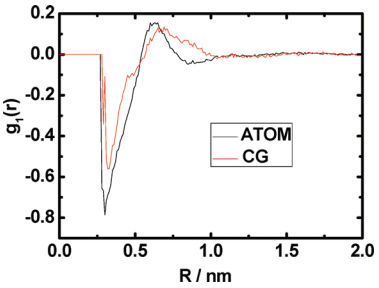

Figure 6. Orientational correlation functions $g_1(r)$ as a function of the distance between the centers of mass of the CN groups from atomistic MD or between CN beads from CG MD (with 6P model) simulations at 300 K.

distance, which is quite similar to our atomistic simulation result, indicating that the most favorable geometrical arrangement between the nearest-neighboring molecules in the CG simulation is also antiparallel, too, which is slightly beyond our expectation. We have demonstrated that this arrangement originates from the Coulombic interactions, which are essentially determined by the presence of the polar CN groups.[61] Although in our CG model, the dipolar interactions are not considered explicitly, the CG force field is constructed in a way to reproduce the structural features of the underlying atomistic model; thus, the local structure information associated with the electrostatic interactions is already incorporated into the nonbonded interaction parameters of CN. Moreover, this antiparallel arrangement demonstrates again the validity of the CG 6P model and optimized FF parameters.

These results suggest that the 6P model is the most appropriate CG model compared with the other two. There are several possible explanations for the failure to obtain a stable nematic phase with the 5P and the 7P models. First, the simplification of representing *a benzene ring in which all atoms are in the same plane* as a spherical C6 bead (i.e., in 5P) or two spherical P3 beads (i.e., in 7P) is unable to realistically account for the excluded volume of the biphenyl mesogenic unit in the 5CB molecule. According to Onsager's theory, excluded volume effect could have a large effect on the stability of nematics.[62] This inability to represent the true excluded volume is, however, one of the inevitable consequences of the coarse-graining technique, wherein groups of atoms are lumped together into a single spherical CG bead. Although one can mimic the true excluded volume "shape" of the biphenyl mesogenic unit as close as possible by varying the bead number or bead size based on the atomic architecture as we did for the 6P model, the necessary simplifications inherent in the creation process of a CG model often weaken the close connections to the underlying atomistic representation. Thus, certain discrepancies (i.e., pair distributions as shown in Figure 4) at the level of local packing between the atomistic and the CG description can be expected, which may even cause some of the physical properties (i.e., LC structure formation) not to be reproduced at the CG level. Apparently, any CG representation is nonoptimal compared with an atomistic description, and designing a mapping scheme is thus an optimization problem.[34] So far no unique answer is available for the CG mapping. A very careful development of CG models is generally required such that they can represent as faithfully as possible the true excluded volume shape of the given molecule. Second, although the intramolecular constraints are used to preserve the overall size of the rigid biphenyl unit during the coarse grain construct, the measured shape anisotropy of the biphenyl segment is different for the three CG models. For example, the 7P model has a larger length-to-width ratio of κ = 2.6, due to the mapping of one benzene ring into two P3 beads with a small excluded volume diameter σ. But the κ values for 5P and 6P are very close to each other and about 2.1, also in agreement with the atomistic data. It should be noted that, in addition to excluded volume, the shape anisotropy is a fundamental feature necessary for the formation of liquid crystal phases according to Onsager's theory.[62] Recent simulations of Brown[63] showed that the Gay–Berne model with a lower values of κ can form isotropic, nematic, and smectic phases, whereas the nematic phase becomes thermodynamically unstable at higher κ. Indeed the very similar conclusions were drawn from the simulations of other LC model systems including spherocylinders and rods. Too much shape anisotropy destroys the nematic phase completely. Again, this reason may lead the 7P model to have no chance to reproduce a stable nematic phase at the given temperature of 300 K and pressure of 1 atm. Third, as for the 5P model, although its rigid biphenyl unit has the same shape anisotropic ratio as in the 6P model, C6 beads in the 5P model can pack more tightly than in the 6P model, as evidenced by a stronger nearest-neighbor peak along with several small peaks in the RDF of Figure S2(d) in the Supporting Information. It should be noted that unlike the 6P model the 5P model system at 300 K and 1 atm forms into the smectic phase, which allows for a locally very tight packing of rigid biphenyl units. Since CG beads play the role of a space-filling particle, the size of the beads and the "softness" of their interaction potential could greatly affect the packing. Note that the rigid biphenyl unit includes two big C6 beads in the 5P model, but one big C6 bead and two small P3 beads in the 6P model. And we choose the Lennard-Jones (LJ) 9–6 potential for the nonbonded interaction. Although, as already mentioned before, we are unable to completely reproduce the correct packing with the CG model, this high packing in the 5P model still points to an effect due to the use of soft LJ interactions, which enhances the overlapping of CG beads. In general, to properly reproduce the real local packing with a larger CG particle, a pair potential with the steeper repulsion term is required. As a whole, the use of the 5P or 7P model as a description of a real 5CB LC molecule has some obvious limitations.

Our results show that small differences in the CG mapping schemes have significant consequences for the results of the CG simulations. As the model always plays a crucial role in the resulting local structural properties and phase stability, to design a reliable model it is important to properly preserve the geometrical shape, size, and the true excluded volume shape of the given molecule in the coarse grain construct. To further verify the validity of the 6P model, we will use the 6P model with the corresponding FF to study the NI phase transition and dynamics of 5CB in the subsequent sections.

3.2. NI Phase Transition Temperature (T_{NI}). Figure 5 shows the evolution of the order parameter P_2 at temperatures between 300 and 320 K for CG simulations of the 6P model system. At 305 K, P_2 goes down first and then increases at the time of 200 ns and finally fluctuates around 0.4. The averaged order parameter, $\langle P_2 \rangle$, over the last 200 ns is about 0.41, indicating the formation of the nematic phase. At T = 310 K, the value of P_2 fluctuates between 0 and 0.2, suggesting the formation of an isotropic phase. Clearly, the critical temperature of NI transition of our 6P model should be between 305 and 310 K, which is the same as our previous atomistic simulation[18] and very close to the experimental value of 306.7[10] or 308 K.[11]

dx.doi.org/10.1021/jp210764h | J. Phys. Chem. B 2012, 116, 2075–2089

This illustrates that, although the current CG force field is parametrized at 300 K, it is valid for the temperature range we studied; hence, the 6P model can display the NI phase transition almost at the same temperature and pressure as the underlying atomistic model.

Meanwhile, the presence of the NI phase transition can be revealed by the temperature-dependent averaged order parameter and density. Figure 7 plots the averaged densities and $\langle P_2 \rangle$ derived from atomistic and CG simulations at different temperatures, together with several sets of the experimental densities. As for P_2, the CG model shows quite similar temperature dependence to the underlying atomistic model. As presented in Figure 7, at the isotropic−nematic transition both CG results and atomic data exhibit a jump of P_2, in agreement with the weak first-order nature of the IN transition.[18] More importantly, the CG calculated P_2 is very close to the atomistic simulated one and the accord of the CG simulated T_{NI} with the atomistic simulated and the experimental ones (dot lines) is quite good, indicating again that our 6P model and the associated CG FF is accurate enough to predict the IN transition rather similar to the actual one.

As for the density, our 6P model produces densities not only comparable with the corresponding experimental data with the underestimation of less than 2% but also close to atomistic simulated values with a density underestimation by a factor of 3.5%, which further confirms the good quality of our 6P model and the associated CG FF. Moreover, the 6P model shows a quite similar temperature dependence to the underlying atomistic model; that is, the density does not present a sharp discontinuity at the isotropic−nematic transition in Figure 7,

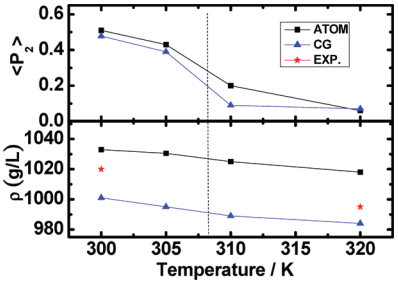

Figure 7. Order parameters (top) and averaged densities (bottom) for the atomistic 5CB system and CG 6P model system as a function of temperature. Some available experimental densities are also presented. The vertical dash line corresponds to the T_{NI} in the experiment.[10,11]

which is also in agreement with the weak first-order nature of the NI transition;[64] i.e., NI transition sometimes cannot be absolutely discrete by the densities.

In short, by combining the structure-based and thermodynamic quantities-based methods for the parametrization of CG interaction potentials and attempting to use several fragment molecular systems to derive the CG nonbonded interaction parameters, the derived CG potentials are not only thermodynamically and structurally consistent with the underlying atomistic model but also maintain transferability at least to some extent. Consequently, there is excellent consistency in the transition temperature, the structure, and thermodynamic properties of the phases formed and the transition order among these CG and atomistic MD studies.

3.3. Dynamics. In addition to the thermodynamic and structural properties, we also extend the validation process of our 6P model and the associated FF to the dynamic properties of the 5CB. So far, no CG model has been parametrized to quantitative modeling of diffusion or other dynamic behavior. Additionally, it is well-known that the anisotropic diffusion of the nematic phase is anisotropy. So, it is quite interesting to study this special property using the 6P model and the FF parameters. As shown in Table 7, in the nematic phase at 300 K, $D_{\parallel}$ (parallel to the director) is larger than $D_{\perp}$ (perpendicular to the director), yielding the expected diffusion anisotropy with the ratio $D_{\parallel}/D_{\perp}$ = 2.3, which is close to the experimental value measured for 5CB ($D_{\parallel}/D_{\perp}$ = 2.44). Most interesting, the CG simulated values of $D_{\parallel}$ and $D_{\perp}$ agree reasonably with the experimental data,[14] and this agreement is even better than those for the united atomistic simulations.[18] Note that the accelerated dynamics, arising from the softer CG nonbonded interaction potentials and the reduction of the number of degrees of freedom, which usually appears in the process of CG simulation,[23,24,65] is not seen in our CG MD simulations. The possible reason for this lies in the excluded volume effect, wherein the presence of a big spherical C6 bead in the 6P model, as evidenced by a higher nearest-neighbor peak along with a relatively larger peak position in the RDF of Figure 4 c when compared to the underlying atomistic representation, slows down the translational movements. Thus, the computed diffusion coefficients for the 6P model are more closely matched to the experimental values than atomistic simulated data. Furthermore, the diffusion coefficient in the isotropic phase was calculated. As listed in Table 7, the resulting D_{iso} = 8 × 10^{-11} m^2/s for the 6P model at 310 K is also very close to the reported experimental value of 6 × $10^{-11}$$m^2/s$. In particular, similar to that obtained from an atomistic molecular dynamics calculation, the CG simulated D_{iso} at 310 K are also slightly smaller than $D_{\parallel}$ at 300 K, which follows the experimental behavior of $D_{\parallel} > D_{iso}$ near the NI transition.[14] As mentioned before, due to the use of a larger time step in integrating the equations of motion and reduced presentation, the CG simulation is at least 30 times faster than the corresponding atomistic simulation in achieving the same total simulation time, suggesting CG simulation is indeed a promising tool in the study of LC phase transitions that typically occur on larger systems at longer time scales.

Table 7. Comparison of Diffusion Coefficients between United Atomistic and CG Simulations (6P Model) and Experimental Values for the 5CB System

translational diffusion coefficients	temp (K)	united atomistic simulation[18]	CG simulation	expt[14]
$D_{\parallel}$ (10^{-11} m^2/s)	300	14.6	8.2	6.6
$D_{\perp}$(10^{-11} m^2/s)	300	6.3	3.6	2.7
$D_{\parallel}/D_{\perp}$	300	2.3	2.3	2.4
D_{iso} (10^{-11} m/s)	310	14.1	8.0	6.0

4. CONCLUSION

The main focus of the present work is to build a coarse-grained model for the liquid crystalline 5CB molecule that enables MD simulation study of phase behavior currently almost inaccessible by atomistic models. To reproduce the phase behavior of the 5CB system accurately, a reasonable mapping scheme and an optimal force field are needed. Since the mapping of the atomistic structure to the CG model is not unique but at the same time very crucial in terms of both predicting power and efficiency, three different but closely related CG models, i.e., 5P,

dx.doi.org/10.1021/jp210764h | J. Phys. Chem. B 2012, 116, 2075−2089

6P, and 7P, are proposed in order to determine the optimal model through comparisons on their abilities in reproducing the specific properties under investigation. Indeed, our choice of these three particular CG models is helpful to understand how the difference in mapping schemes affects the performance of the CG models. So far, few studies have been pursued with the aim to design mapping schemes and learn something about their capacities.

Meanwhile, as the CG force field parametrization is a crucial step, which determines the predicting power of CG models, devising a careful guideline is thus important for reaching reliable interaction parameters. Note that our step-by-step approach to construct the CG force field is significantly different from previous methods. For the intramolecular bonded interactions, the bond and angle distributions of the 5CB bulk phase are used as the target properties. For the nonbonded interactions between CG particles, we combine the aforementioned structure-based and thermodynamic quantities-based methods for the parametrization of CG interaction potentials and attempt to use several fragment molecular systems to derive the CG nonbonded interaction parameters in order to maintain the transferability of our CG models to some extent. We fix the optimal nonbonded LJ parameters between CG bead pairs such that the results from CG simulations not only correctly reproduce the experimental density and the nematic LC state at 300 K and 1 atm but also reasonably approximate the local structural properties (i.e., RDFs) calculated from underlying atomistic model. Currently there is considerable interest in optimizing the coarse-grained potential to reproduce multiproperties (e.g., several key structural and thermodynamic properties) with the aim to design a coarse-grained model which is thermodynamically and structurally consistent, since this consistency is of great importance for bridging between the different scales in a multiscale simulation.

By analysis and comparison of the performance of the proposed three different CG models with respect to reproducing the density, RDFs, and the nematic phase observed in experiments and atomistic simulations at 300 K and 1 atm, the 6P model is found to be superior over the other two CG models. In particular, the nearest-neighboring molecules are antiparallel to each other in the 6P model, in good agreement with our atomistic simulation, although the dipolar interactions are not considered directly in the CG model. These results illustrate that small differences in the CG mapping schemes have significant consequences for the results of the CG simulations. To design a reliable CG model is important to properly preserve the geometrical shape, size, and the true excluded volume shape of the given molecule in the coarse grain construct. To further verify the validity of the 6P model, we use this model to study the nematic to isotropic (NI) phase transition temperature as well as the diffusion coefficients. There is excellent consistency in the transition temperature, the structure, and the thermodynamic properties of the phases formed, and the transition order among these CG and atomistic MD studies as well as experimental results. This illustrates that, although the current CG force field is parametrized at 300 K, it maintains transferability to some extent and is valid at least for the temperature range we studied. Most important, although no CG model has been so far parametrized to quantitatively model the diffusion or other dynamic behavior, our 6P model can well reproduce the diffusion properties in the 5CB.

From these results, we can conclude that the coincidence of CG results with atomistic MD studies as well as the experimental data validates the rationality of our constructed 6P model and developed FF parameters for 5CB in this work. Its effectiveness to quantitatively model the nCB series and molecules with similar chemical structures is expected.

■ ASSOCIATED CONTENT

Supporting Information

Comparison of RDFs of CG particles C3, C2, CN, P3, and C6 between CG and atomistic simulations of octadecane, hexane, benzonitrile, biphenyl, and hexylbiphenyl systems, the comparison of RDFs of CG particles C2, C3, CN, and C6 between CG (5P model) and atomistic simulations, as well as the CG bond stretching and bond angle interactions parameters for the dodecane, benzene, and butyronitrile molecules. This material is available free of charge via the Internet at http://pubs.acs.org.

■ AUTHOR INFORMATION

Corresponding Author

*Email: hxguo@iccas.ac.cn.

Notes

The authors declare no competing financial interest.

■ ACKNOWLEDGMENTS

We are grateful for the support of the NSF of China (20874110 and 20674093). We also thank the supercomputing center of CAS for supporting computing resources.

■ REFERENCES

(1) Sato, O.; Kubo, S.; Gu, Z. Z. *Acc. Chem. Res.* **2009**, *42*, 1−10.
(2) Musevic, I.; Skarabot, M.; Tkalec, U.; Ravnik, M.; Zumer, S. *Science* **2006**, *313*, 954−958.
(3) Kempe, M. D.; Scruggs, N. R.; Verduzco, R.; Lal, J.; Kornfield, J. A. *Nat. Mater.* **2004**, *3*, 177−182.
(4) Lago, S.; Gamez, F.; Cortada, M.; Merkling, P. J.; Garzon, B. *J. Phys. Chem. B* **2008**, *112*, 8069−8075.
(5) Coles, H. J.; Strazielle, C. *Mol. Cryst. Liq. Cryst.* **1979**, *55*, 237−250.
(6) Brake, J. M.; Daschner, M. K.; Luk, Y. Y.; Abbott, N. L. *Science* **2003**, *302*, 2094−2097.
(7) Holmes, C. J.; Cornford, S. L.; Sambles, J. R. *Appl. Phys. Lett.* **2009**, *95*, 171114.
(8) Blanc, C.; Svensek, D.; Zumer, S.; Nobili, M. *Phys. Rev. Lett.* **2005**, *95*, 97802.
(9) Lapointe, C. P.; Mason, T. G.; Smalyukh, I. I. *Science* **2009**, *326*, 1083−1086.
(10) Oweimreen, G. A.; Morsey, M. A. *Thermochim. Acta* **2000**, *346*, 37−47.
(11) Mansare, T.; Decressain, R.; Gors, C.; Dolganov, V. K. *Mol. Cryst. Liq. Cryst.* **2002**, *382*, 97−111.
(12) Kobinata, S.; Kobayashi, T.; Yoshida, H.; Chandani, A. D. L.; Maeda, S. *J. Mol. Struct.* **1986**, *146*, 373−382.
(13) Sandmann, H.; Hamann, F.; Wurflinger, A. *Z. Naturforsch.* **1997**, *52*, 739.
(14) Dvinskikh, S. V.; Furo, I. *J. Chem. Phys.* **2001**, *115*, 1946−1950.
(15) Komolkin, A. V.; Laaksonen, A.; Maliniak, A. *J. Chem. Phys.* **1994**, *101*, 4103−4116.
(16) Cross, C. W.; Fung, B. M. *J. Chem. Phys.* **1994**, *101*, 6839−6848.
(17) Cacelli, I.; Prampolini, G.; Tani, A. *J. Phys. Chem. B* **2005**, *109*, 3531−3538.
(18) Zhang, J.; Su, J.; Guo, H. *J. Phys. Chem. B* **2011**, *115*, 2214−2227.
(19) Izvekov, S.; Voth, G. A. *J. Phys. Chem. B* **2005**, *109*, 2469−2473.
(20) Marrink, S. J.; Risselada, H. J.; Yefimov, S.; Tieleman, D. P.; de Vries, A. H. *J. Phys. Chem. B* **2007**, *111*, 7812−7824.
(21) Srinivas, G.; Klein, M. L. *Nanotechnology* **2007**, *18*, 205703.

(22) Shelley, J. C.; Shelley, M. Y.; Reeder, R. C.; Bandyopadhyay, S.; Moore, P. B.; Klein, M. L. *J. Phys. Chem. B* **2001**, *105*, 9785−9792.
(23) Harmandaris, V. A.; Adhikari, N. P.; van der Vegt, N. F. A.; Kremer, K. *Macromolecules.* **2006**, *39*, 6708−6719.
(24) Harmandaris, V. A.; Reith, D.; Van der Vegt, N. F. A.; Kremer, K. *Macromol. Chem. Phys.* **2007**, *208*, 2109−2120.
(25) Muller-Plathe, F. *Chemphyschem* **2002**, *3*, 754−769.
(26) Reith, D.; Putz, M.; Muller-Plathe, F. *J. Comput. Chem.* **2003**, *24*, 1624−1636.
(27) Srinivas, G.; Discher, D. E.; Klein, M. L. *Nat. Mater.* **2004**, *3*, 638−644.
(28) Milano, G.; Goudeau, S.; Müller-Plathe, F. *J. Polym. Sci. Part A: Polym. Phys.* **2005**, *43*, 871−885.
(29) Milano, G.; Müller-Plathe, F. *J. Phys. Chem. B* **2005**, *109*, 18609−18619.
(30) Li, X.; Ma, X.; Huang, L.; Liang, H. *Polymer* **2005**, *46*, 6507−6512.
(31) Li, X.; Kou, D.; Rao, S.; Liang, H. *J. Chem. Phys.* **2006**, *124*, 204909.
(32) Van Der Vegt, N. F. A.; Peter, C.; Kremer, K. Structure-based coarse-and fine-graining in soft matter simulations. In *Coarse-Graining of Condensed Phase and Biomolecular Systems*; Voth, G. A., Ed.; CRC Press, Taylor and Francis Group: New York, 2009; p 379.
(33) Lyubartsev, A. P.; Laaksonen, A. *Phys. Rev. E* **1995**, *52*, 3730−3737.
(34) Peter, C.; Kremer, K. *Soft Matter* **2009**, *5*, 4357−4366.
(35) Izvekov, S.; Voth, G. A. *J. Chem. Phys.* **2005**, *123*, 134105.
(36) Srinivas, G.; Klein, M. L. *Mol. Phys.* **2004**, *102*, 883−889.
(37) Monticelli, L.; Kandasamy, S. K.; Periole, X.; Larson, R. G.; Tieleman, D. P.; Marrink, S. J. *J. Chem. Theory Comput.* **2008**, *4*, 819−834.
(38) Lopez, C. A.; Rzepiela, A. J.; de Vries, A. H.; Dijkhuizen, L.; Hunenberger, P. H.; Marrink, S. J. *J. Chem. Theory Comput.* **2009**, *5*, 3195−3210.
(39) Peter, C.; Kremer, K. *Faraday Discuss.* **2009**, *144*, 9−24.
(40) Allen, E. C.; Rutledge, G. C. *J. Chem. Phys.* **2008**, *128*, 154115.
(41) Allen, E. C.; Rutledge, G. C. *J. Chem. Phys.* **2009**, *130*, 204903.
(42) Muller-Plathe, F. *Soft Mater.* **2003**, *1*, 1−31.
(43) Peter, C.; Kremer, K. *Faraday. Discuss.* **2010**, *144*, 9−24.
(44) Peter, C.; Delle Site, L.; Kremer, K. *Soft Matter* **2008**, *4*, 859−869.
(45) Nielsen, S. O.; Lopez, C. F.; Srinivas, G.; Klein, M. L. *J. Chem. Phys.* **2003**, *119*, 7043−7049.
(46) Lopez, C. F.; Nielsen, S. O.; Srinivas, G.; DeGrado, W. F.; Klein, M. L. *J. Chem. Theory Comput.* **2006**, *2*, 649−655.
(47) Peter, C.; Kremer, K. *Soft Matter* **2009**, *5*, 4357−4366.
(48) Lorentz, H. A. *Ann. Phys.* **1881**, *12*, 127.
(49) Rossini, F. D. *Selected Values of Physical and Thermodynamic Properties of Hydrocarbons and Related Compounds: Comprising the Tables of the American Petroleum Institute Research Project 44 Extant as of December 31, 1952*; Published for the American Petroleum Institute by Carnegie Press, New York, 1953.
(50) Egloff, G. *Physical Constants of Hydrocarbons*; Reinhold Pub. Corp.: New York, 1939; Vol. *1*.
(51) Hess, B.; Kutzner, C.; van der Spoel, D.; Lindahl, E. *J. Chem. Theory Comput.* **2008**, *4*, 435−447.
(52) Martin, M. G.; Siepmann, J. I. *J. Phys. Chem. B* **1998**, *102*, 2569−2577.
(53) Martin, M. G.; Siepmann, J. I. *J. Phys. Chem. B* **1999**, *103*, 4508−4517.
(54) Wick, C. D.; Martin, M. G.; Siepmann, J. I. *J. Phys. Chem. B* **2000**, *104*, 8008−8016.
(55) Wick, C. D.; Stubbs, J. M.; Rai, N.; Siepmann, J. I. *J. Phys. Chem. B* **2005**, *109*, 18974−18982.
(56) Maerzke, K. A.; Schultz, N. E.; Ross, R. B.; Siepmann, J. I. *J. Phys. Chem. B* **2009**, *113*, 6415−6425.
(57) Nose, S. *Mol. Phys.* **1984**, *52*, 255−268.
(58) Hoover, W. G. *Phys. Rev. A* **1985**, *31*, 1695−1697.
(59) Parrinello, M.; Rahman, A. *J. Appl. Phys.* **1981**, *52*, 7182−7190.
(60) Luckhurst, G. R.; Veracini, C. A. E. *The Molecular Dynamics of Liquid Crystals*; Springer: New York, 1994; Vol. *431*.
(61) Pelaez, J.; Wilson, M. *Phys. Chem. Chem. Phys.* **2007**, *9*, 2968−2975.
(62) Onsager, L. *Ann. N.Y. Acad. Sci.* **1949**, *51*, 627−659.
(63) Brown, J. T.; Allen, M. P.; del Rio, E. M.; de Miguel, E. *Phys. Rev. E* **1998**, *57*, 6685.
(64) Miguel, E. d.; Rio, E. M. d.; Brown, J. T.; Allen, M. P. *J. Chem. Phys.* **1996**, *105*, 4234−4249.
(65) Praprotnik, M.; Matysiak, S.; Delle Site, L.; Kremer, K.; Clementi, C. *J. Phys.: Condens. Matter* **2007**, *19*, 292201.